Optics and Lasers in Engineering 50 (2012) 1757–1764

Contents lists available at SciVerse ScienceDirect

Optics and Lasers in Engineering

journal homepage: www.elsevier.com/locate/optlaseng

The study on microscopic mechanical property of polycrystalline with SEM moiré method

Yanjie Li [a,b], Huimin Xie [a,*], Minjin Tang [a], Jianguo Zhu [a], Qiang Luo [c], Changzhi Gu [c]

[a] AML, Department of Engineering Mechanics, Tsinghua University, Beijing 100084, China
[b] School of Civil Engineering and Architecture, University of Jinan, Jinan 250022, China
[c] Institute of Physics, Chinese Academy of Sciences, Beijing 100190, China

ARTICLE INFO

Article history:
Received 30 March 2012
Received in revised form
2 June 2012
Accepted 6 July 2012
Available online 9 August 2012

Keywords:
SEM moiré
Grain boundary
Deformation
Random phase shifting

ABSTRACT

The local microscopic deformation of polycrystalline low carbon steel under uniaxial tension is measured through SEM moiré method. In order to produce high frequency gratings, focused ion beam (FIB) milling is used due to its direct writing capability. With gratings of 2000 lines/mm, the variations of SEM moiré fringes with the increase of stress around a triple point of grain boundary and inside a grain are observed respectively and it is found that we can tell whether the specimen has yielded by moiré fringes. With gratings of 5000 lines/mm, SEM moiré fringes around five different types of grain boundaries are recorded and analyzed with random phase shifting algorithm. By observing the strain fields around different types of grain boundaries, it is found that the deformation fields around these grain boundaries are inhomogeneous and increase with stress. However, the strain distributions are different, which is probably related with the angle between the loading direction and the grain boundary and the misorientation of two adjacent grains. It is also found that the inhomogeneous strain is caused by slip and the bending direction of moiré fringes is in agreement with the direction of slip band.

1. Introduction

Most metallic materials are polycrystalline formed by a collection of fine grains on the order of 100 μm or even smaller. Therefore, it is reasonable and accurate enough to consider the material as homogeneous and isotropic at the macroscopic scale. However, it is increasingly evident that local microstructural effects cannot be ignored at the microscopic scale, such as grain boundary, grain size, grain shape and crystallographic texture. Microstructure-based models like crystal plasticity models have been developed to predict the microscopic mechanical response of polycrystalline material. However, the accurate applications of these models are still currently limited to a narrow range of circumstances. Developing more accurate models will require an improved understanding of deformation mechanisms at the grain level, which will, in turn, require grain level experiments that give quantitative measurements on a full field basis.

The applicable experimental methods for quantitative, full-field, grain level measurements are digital image correlation (DIC) [1–4], grid technique [5], moiré interferometry [6] and SEM moiré method [7,8]. DIC makes use of the gray intensity to calculate the full field displacement by correlating the images captured before and after deformation. It is based on an assumption that the gray intensity of each point before and after deformation is constant. In other words, this method does not allow the obvious changes on specimen surface; otherwise, only the relative deformation between adjacent stages, not the real deformation, can be directly calculated. The grid technique has been proven to work well for large amounts of global strain (on the order of unity). Moiré interferometry is successfully utilized to measure polycrystalline Al with large grain sizes on the millimetric scale [6]. However, due to its limitation of spatial resolution, moiré interferometry does not apply to the deformation analysis of grain at micron-scale or smaller. Compared to the above mentioned methods, SEM moiré method possesses three major advantages: (1) insensitive to the surface changes; (2) high displacement sensitivity up to 0.1 μm; (3) high spatial resolution. Therefore SEM moiré method is well suited to analyze the full field deformation of polycrystalline with fine grains.

Grating fabrication and fringes analysis are two critical steps for all kinds of moiré methods and SEM moiré method is no exception. For microstructural deformation analysis, gratings of frequency higher than 1000 lines/mm are required. As reported, there are four available fabrication techniques for such high frequency gratings, including holographic photolithography [9], electron beam lithography (EBL) [10], nano-imprint technology

* Corresponding author. Fax: +86 10 62781824.
E-mail address: xiehm@mail.tsinghua.edu.cn (H. Xie).

0143-8166/$ - see front matter © 2012 Elsevier Ltd. All rights reserved.
http://dx.doi.org/10.1016/j.optlaseng.2012.07.004

[11] and focused ion beam (FIB) milling [12,13]. The process of holographic photolithography is relatively cumbersome, which consists of coating photoresist, exposure, developing, depositing metal film and removing the rest of photoresist. This technique can produce gratings very quickly and the size is usually a few tens of millimeters. The disadvantages lie in the high precision demand of optics setup and vibration isolation. The process of EBL is almost the same as photolithography except that the exposure source is electron beam instead of laser beam and the grating pattern is formed by pattern generator instead of the interference of two laser beams. Nano-imprint technology requires a high precision mold, which is expensive. This technique involves an imprint step with physical deformation of a thin film of a thermoplastic polymer cast on a substrate using a rigid mold under pressure and elevated temperature above the glass transition temperature (T_g), followed by solidification and demoulding after the polymer cooled to a temperature below T_g. Compared to the other three methods, FIB milling is a more straightforward technique (maskless and resistless) to directly write the grating on a specific region of the specimen surface. Both FIB and EBL allow producing grids with frequencies up to 10,000 lines/mm, but they are time consuming and of low throughput due to the serial nature of the process. Thus neither is suited for large scale patterning. Besides, the size of the processed sample is limited by the size of the vacuum chamber. Therefore the grating made by EBL and FIB is more suitable to measure microscopic deformation. In this study, FIB is selected due to its direct writing capability on a specific site.

With regard to fringes analysis, fringe centering technique [14], which consists of filtering, fringe centerline detection, binerization, peak detection, fringe thinning, fringe orders assignment and fractional fringe order calculation, is adopted in most previous studies on SEM moiré. This manually handling technique only makes use of the information of fringes on integral order, which leads to a lower displacement measurement precision. It is well known that phase shifting technique not only can realize automatic processing of moiré fringes, but also can enhance the displacement precision. Although four-step phase shifting technique has been introduced to SEM moiré method [15], it is not easy to implement this technique unless PZT actuator is introduced since the specimen stage and the electron beam cannot be moved precisely. This difficulty can be overcome by using random phase shifting technique since it does not need to know the precise phase shift step. Wang et al. [16,17] developed an advanced iterative algorithm to obtain the phase shift step and the phase information at the same time using three or more phase shift images. Hu et al. [18] used random phase shifting SEM moiré technique to reconstruct periodic structure. Wang et al. [19] utilized random phase shifting SEM moiré technique to measure residual thermo-creep deformation of copper interconnects.

This work aims at characterizing the local microscopic mechanical property of polycrystalline material by SEM moiré method. The tested object is low carbon steel, Q235B. The principle of SEM moiré method is presented in Section 2 followed by the grating fabrication method in Section 3. Experiments and results are given in Section 4. Finally, conclusions are summarized.

2. SEM moiré method

2.1. Measurement principle of SEM moiré

SEM image is acquired through point by point scanning of electron beam from left to right, from up to down. Therefore the scanning lines can be regarded as a horizontal periodical grid and serve as the reference grating. In principle, SEM scanning moiré is generated by the superposition of the specimen grating and the reference grating with almost identical frequency. When these two groups of grating are parallel, the formed moiré is called as parallel moiré; otherwise, it is called as rotational moiré, see Fig. 1.

Moiré fringes are isothetic lines of displacement [20]. Therefore, the displacement field and the strain field can be obtained by analyzing the fringes. Phase shifting moiré method not only avoids the cumbersome of the fringe centering method [14] and realizes the automatic processing of fringes, but also improves the displacement accuracy since it makes full use of the gray information of each point. Conventional phase shifting algorithms require the phase shift amounts to be known. However, it is difficult to meet this requirement in SEM moiré as the specimen stage or the electron beam cannot be moved precisely on submillimeter scale. To overcome this difficulty, random phase shifting SEM moiré method is used in this paper. It consists of two steps. First, record random phase shifting moiré fringes under SEM by finely shifting the electron beam. Second, analyze the recorded moiré fringes with an advanced iterative algorithm proposed by Wang et al. [16,17]. The proposed algorithm is based on the least-squares iterative algorithm and has been proved effective for any three or more images with completely random phase shifts. In this approach, both phase shift amounts and wrapped phase distributions, $\phi(x,y)$, are treated as unknowns and they are determined simultaneously through an iteration process, including pixel-by-pixel iteration to determine phase distribution, frame-by-frame iteration to determine phase shifts and check out the convergence limit. The algorithm repeats these two previous steps until the phase-shift values converge.

An unwrapping procedure is required to obtain the unwrapped phase, $\phi'(x,y)$. The relationship between the unwrapped phase, $\phi'(x,y)$, and the displacement, $v(x,y)$, is

$$\phi'(x,y) = \frac{2\pi}{p_r} v(x,y) \quad (1)$$

where p_r is the pitch of the reference grating, $v(x,y)$ is the displacement of the specimen grating relative to the reference grating along the principal direction of the reference grating, y.

The strain in direction y can be expressed by

$$\varepsilon(x,y) = \frac{p_r}{2\pi} \frac{\partial \phi'(x,y)}{\partial y} \quad (2)$$

In the tensile test, under a constant tensile load, translate the scanning lines three times along y direction to acquire four fringes images, as shown in Fig. 2(a). The translation amount is unknown but less than p_r each time. Using the random phase shifting algorithm, the wrapped phase field can be got from these four

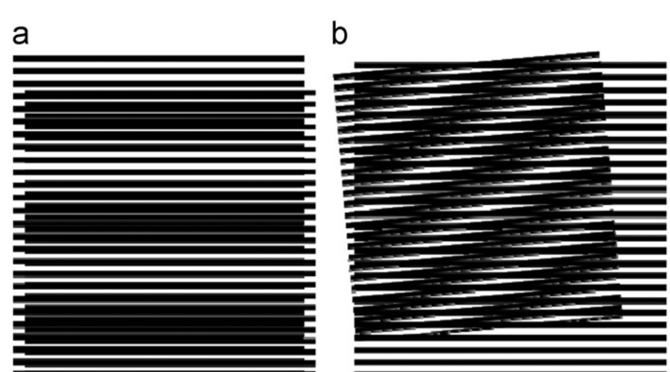

Fig. 1. Formation of moiré fringes. (a) Parallel moiré (b) Rotational moiré.

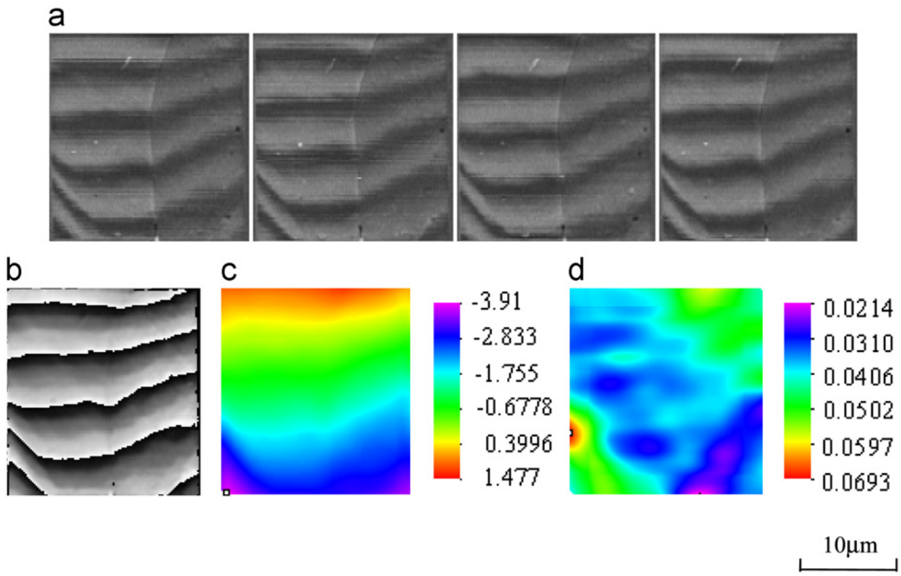

Fig. 2. An example of random phase shifting moire fringes and the calculated results, the dots in (c) and (d) are the locations of the maximum displacement and strain respectively. (a) Four random phase shifting fringes, (b) wrapped phase, (c) displacment field, (d) strain field.

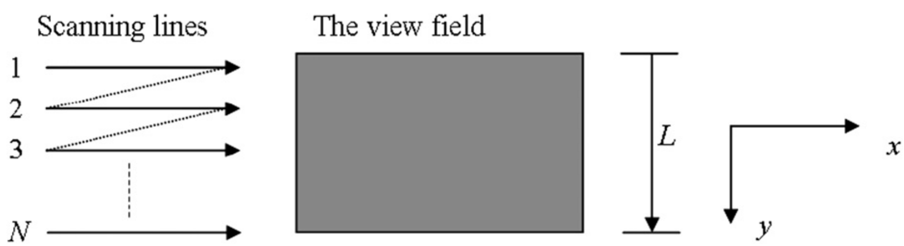

Fig. 3. Diagram of scanning lines and the view field under SEM.

images, as shown in Fig. 2(b). Then the phase field is unwrapped, the full field displacement (Fig. 2(c)) and strain (Fig. 2(d)) can be calculated by the Eqs. (1) and (2).

2.2. Preliminary calibration of the frequency of reference grating

Assume that the scanning lines of SEM is parallel to axis *x*, as shown in Fig. 3, the frequency of reference grating, f_r, is given by

$$f_r = \frac{N}{L} \tag{3}$$

where L is the length of the view filed along axis y and N is the number of scanning lines.

Let L_0 represents the gauge length of the SEM monitor along axis y and M represents magnification, then

$$L = \frac{L_0}{M} \tag{4}$$

Therefore

$$f_r = \frac{N}{L} = \frac{MN}{L_0} \tag{5}$$

Since L_0 is a constant, the frequency of the scanning lines is linearly proportional to the magnification with a specified number of scanning lines. In other words, the frequency of the reference grating can be varied by altering the magnification. To get moiré fringes in an efficient way, the relationship between the frequency of the reference grating and the magnification should be calibrated. The physical size of each pixel is measured by the scale bar and the frequency can be obtained through taking its reciprocal. Capture SEM images at different magnifications and measure the corresponding frequencies of the reference grating. Plot these data points and linearly fit them to obtain the relation expression. Fig. 4 illustrate the relation curves of two SEM systems utilized in our experiments, including Shimadzu S-550 and FEI Siron 400NC. This calibration method also applies to other scanning moiré methods, like AFM moiré, STM moiré, TEM moiré and LSCM moiré.

When the frequency of the specimen grating is equal to that of the scanning lines and their directions are parallel, no fringes will turn out and such case is terminologically called as null field moiré. But a small frequency mismatch will lead to moiré fringes. The larger the mismatch is, the denser the fringes are. According to the above mentioned relation expression between the frequency of the reference grating and the magnification, the magnification M_0 at which null moiré fringes are formed can be derived. It is easy to observe moiré fringes by adjusting magnification around M_0. However, it should be noticed M_0 is just a reference value. Due to the measurement error and the difference of working distance, the real magnification corresponding to null moiré fringes probably is not equal to M_0, but definitely around M_0.

3. Grating fabrication method with FIB

FIB technologies are now widely used as powerful tools in the semiconductor industry mainly for micro/nano-structuring, mask repairing, device modification, failure analysis, integrated circuit debugging and others [21,22]. Using FIB to fabricate specimen

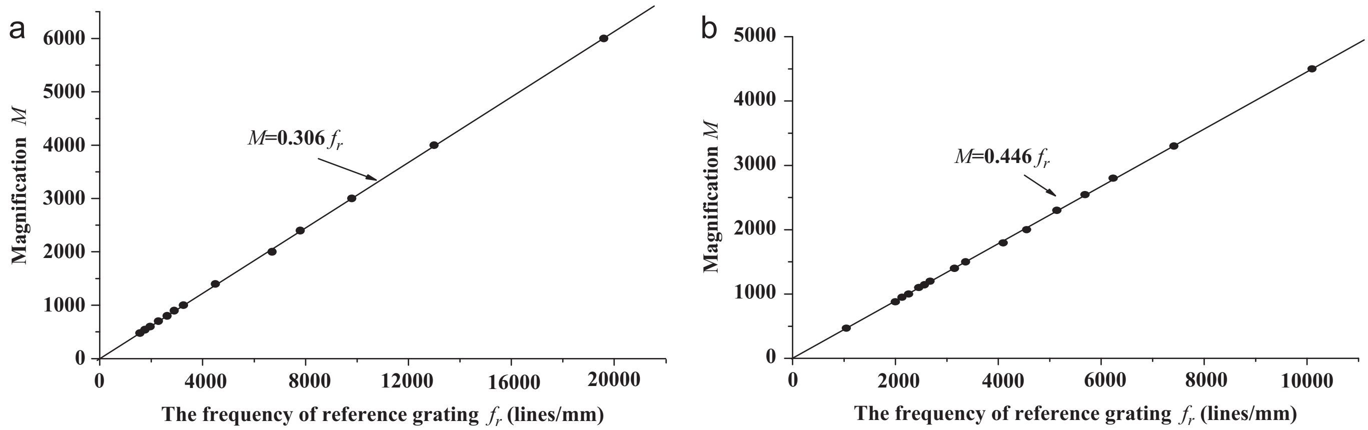

Fig. 4. Calibration of the frequency of reference grating under two SEM systems. (a) Shimadzu S-550, (b) FEI Siron 400NC.

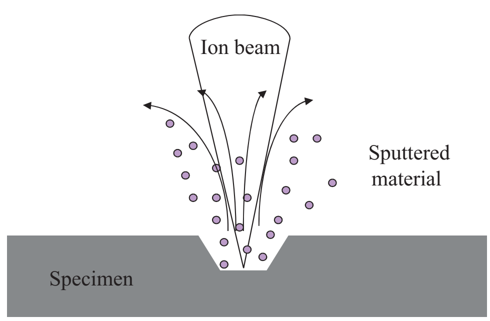

Fig. 5. Diagram of FIB milling.

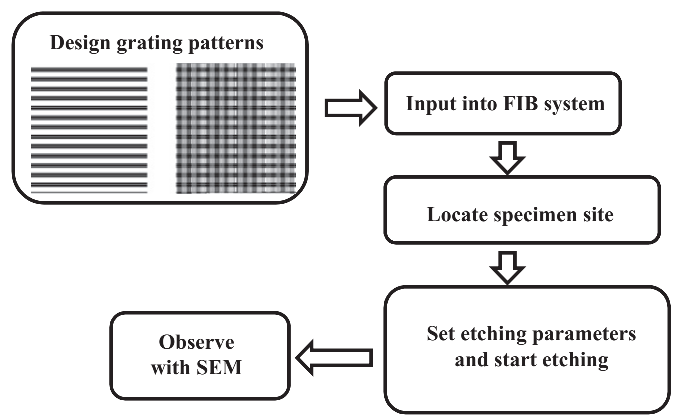

Fig. 6. Flow chart of grating fabrication.

grating, not only extends the application of FIB, but also offers a new tool for moiré method to fabricate grating. FIB milling is achieved by accelerating concentrated ions to a specific site, which etches off any exposed material, leaving a very clean hole [13], as shown in Fig. 5.

A dual beam system (SEM and FIB) is used in the experiments and the flow chart of grating fabrication is shown in Fig. 6. The first step is to design grating patterns and the detail is described in Ref. [13]. Parallel gratings are used to measure one dimensional deformation and cross gratings are used for two dimensional deformation. Then input the designed grating patterns into FIB system and locate the specimen site of interest. Set etching parameters, like the ion beam current and etching depth, and start etching. Finally, observe the fabricated grating with SEM.

In the experiments, parallel specimen gratings of two frequencies are fabricated, as illustrated in Fig. 7. In Fig. 7(a), the frequency is 2000 lines/mm, the gratings are fabricated under Tescan Lyra 3, the ion beam current is 139 pA and the setting etching depth is 1 μm. In Fig. 7(b), the frequency is 5000 lines/mm, the gratings are fabricated under FEI DB 235, the ion beam current is 300 pA and the setting etching depth is 0.5 μm.

4. Experiments and results

Tensile tests are carried out under Shimadzu S-550 and FEI Siron 400NC respectively. The material is low carbon steel, Q235B. To display the grain boundary and fabricate high frequency grating, polish the specimen to a mirror-like plane with sand paper and diamond polishing paste followed by corroding it with a mixed solution of nitric acid and alcohol by volume ratio of 4:100 for 90 s. The boundaries of the grains can be clearly observed under microscope, as shown in Fig. 8. The white part is ferrite and the black part is pearlite. Then fabricate high frequency gratings under dual beam systems, as illustrated in Fig. 7. The principal direction of the specimen grating is parallel to the tensile direction. Finally tensile tests are carried out under scanning electron microscope. Before exerting the load, adjust the principal direction of the specimen grating to be parallel to the principal direction of the reference grating, i.e. the electron beam, by rotating the specimen stage or the electron beam so that parallel moiré fringes can be formed.

4.1. Tensile tests under Shimadzu S-550

The size of the tensile specimen under Shimadzu S-550 is shown in Fig. 9. Since Shimadzu S-550 makes use of Tungsten filament and its resolution is lower compared to field emission scanning electron microscope, the gratings of 2000 lines/mm are used. According to the calibration relationship between the magnification and the frequency of the reference grating, $M=0.306\,f_r$, M_0 should be 612 × . Since the magnification cannot be adjusted continuously, 700 × is adopted to record moiré fringes. Two tensile tests are carried out under Shimadzu S-550 to observe the moiré fringes variation with the increase of the stress around the triple point of grain boundary and in the interior of one grain respectively, as shown in Fig. 10. The stress–strain curve and the moiré fringes corresponding to several stresses are displayed. The stage of yielding can be distinguished clearly through stress–strain curve. It can be seen that, whether around a triple point of grain boundary or in the interior of one grain, the moiré fringes are horizontal, parallel and equally spaced during

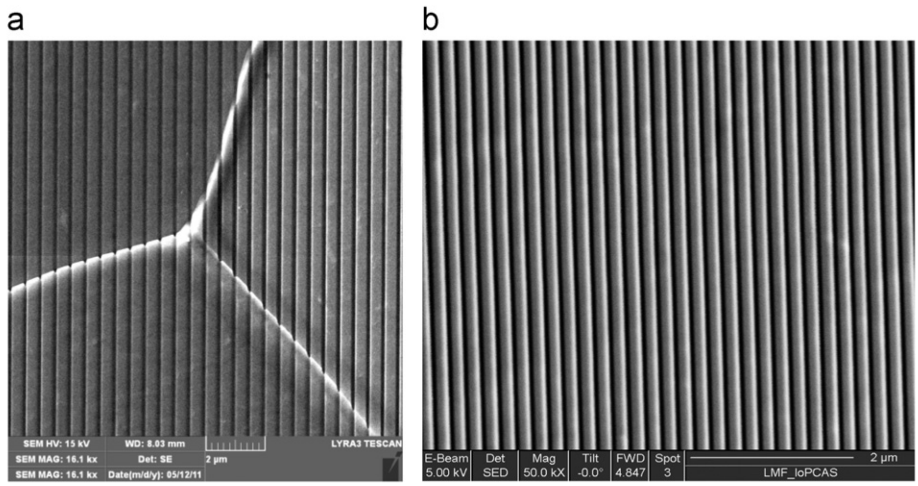

Fig. 7. Parallel specimen gratings. (a) 2000 lines/mm, (b) 5000 lines/mm.

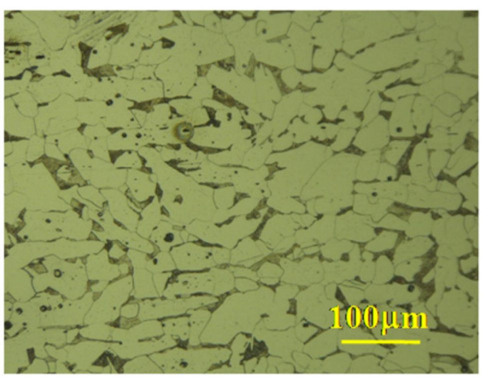

Fig. 8. Microstructure of low carbon steel under optical microscope.

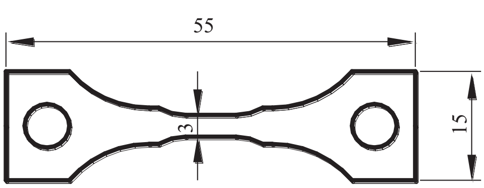

Fig. 9. Size of the tensile specimen under Shimadzu S-550, the unit is mm, the thickness is 0.9 mm.

the stage of elastic deformation; once the specimen is in or has finished the stage of yielding, the moiré fringes become curved and non-uniform. With the increase of the stress, the moiré fringes are more and more curved and denser. Therefore, we can tell whether the specimen has yielded by the variations of moiré fringes. As Shimadzu S-550 makes use of Tungsten filament, its resolution is lower than field emission scanning electron microscope so that the recorded moiré fringes is not as good as those of field emission scanning electron microscope. Therefore, we will quantitatively analyze the influence of the type of grain boundary to the plastic deformation under FEI Siron 400NC.

4.2. Tensile test under FEI Siron 400NC

The size of the tensile specimen under FEI Siron 400NC is shown in Fig. 11. Parallel gratings of 5000 lines/mm are used. Based on the calibration relationship between the magnification and the frequency of the reference grating, $M=0.446\,f_r$, M_0 should be $2230\times$. By adjusting the magnification of scanning electron microscope around M_0, we find that there are no moiré fringes exactly at $2277\times$. In other words, the pitch of the specimen grating is equal to that of reference grating at $2277\times$ before deformation. Therefore, the moiré fringes recorded at $2277\times$ after deformation will correspond to the real deformation of the specimen.

In order to study the influence of different types of grain boundaries to the plastic deformation, five different types of grain boundaries are investigated. Four random phase shifting moiré fringes are captured at one load for each type of grain boundary. Their moiré fringes and the strain fields calculated with random phase shifting algorithm at different stresses are shown in Fig. 12. The dashed lines are grain boundaries. It can be seen that, although with different directions, the deformation fields around these grain boundaries are inhomogeneous and increase with stress. However, the strain distributions are different. In Fig. 12(a), the direction of grain boundary are almost parallel to the loading direction, the grain boundary has no obvious influence on the strain distribution. In Fig. 12(b), the grain boundary is almost perpendicular to the loading direction and the strain around the grain boundary is minimum. There is almost an angle of 45° between the directions of the grain boundaries in Fig. 12(c) and (d) and the loading direction and the strain around the grain boundaries is maximum. Fig. 12(e) correspond to a tricrystal, only the strain around the left grain boundary is minimum and the other two grain boundaries have no obvious influence on the strain distribution. These different distributions are probably caused by the differences of grain orientations around grain boundaries and the different angles between the direction of grain boundaries and the loading direction. The microscopic grain orientations can be detected with Electron backscatter diffraction (EBSD), however, because of severe oxidation, the experiment of EBSD is not successful. The further study will be performed in future.

By observing morphologies of moiré fringes and grating under the stress of 323 MPa corresponding to Fig. 12(d), as shown in Fig. 13, it is found that a slip band appeared in the grating region and the bending direction of moiré fringes is in agreement with the direction of slip band. Therefore, we can tell the direction of slip band according to the bending direction of moiré fringes. At the same time, the moiré fringes become denser around the slip band, which indicates that the inhomogeneous strain is caused by slip.

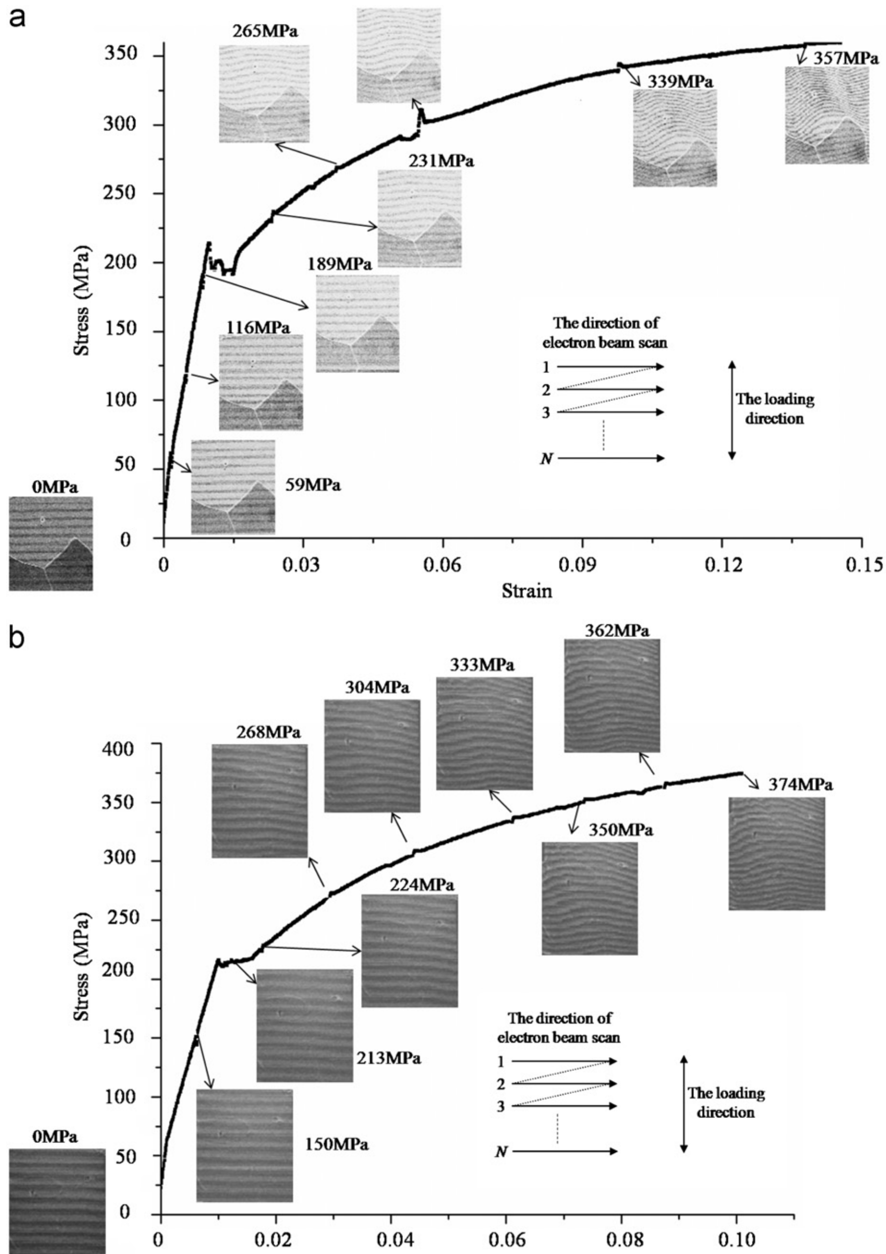

Fig. 10. Variation of moiré fringes with the increase of the stress. (a) Around a triple point of grain boundary, (b) In the interior of one grain.

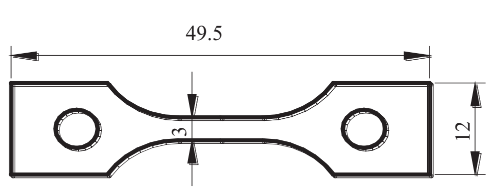

Fig. 11. Size of the tensile specimen under FEI Siron 400NC, the unit is mm, the thickness is 0.9 mm.

5. Conclusions

The local deformation at the microscopic scale of polycrystalline low carbon steel under uniaxial tensile test is studied through SEM moiré method. The grating fabrication technique on metal specimen with FIB milling is presented and the maximum frequency is 5000 lines/mm. With gratings of 2000 lines/mm, the variations of SEM moiré fringes with the increase of stress around a triple point of grain boundary and inside a crystal are observed under Shimadzu S-550 and it is found that whether the specimen has yielded can be distinguished by moiré fringes. With gratings of 5000 lines/mm, SEM moiré fringes around five different types of grain boundaries are recorded under FEI Siron 400NC and analyzed with random phase shifting algorithm. By observing the strain fields around these different types of grain boundaries, it is found that the deformation fields around these grain boundaries are inhomogeneous and increase with stress. However, the strain distributions are different probably as a result of different orientations. The further study is undergoing. It is also found that the inhomogeneous strain is caused by slip and the bending direction of moiré fringes is in agreement with the direction of slip band.

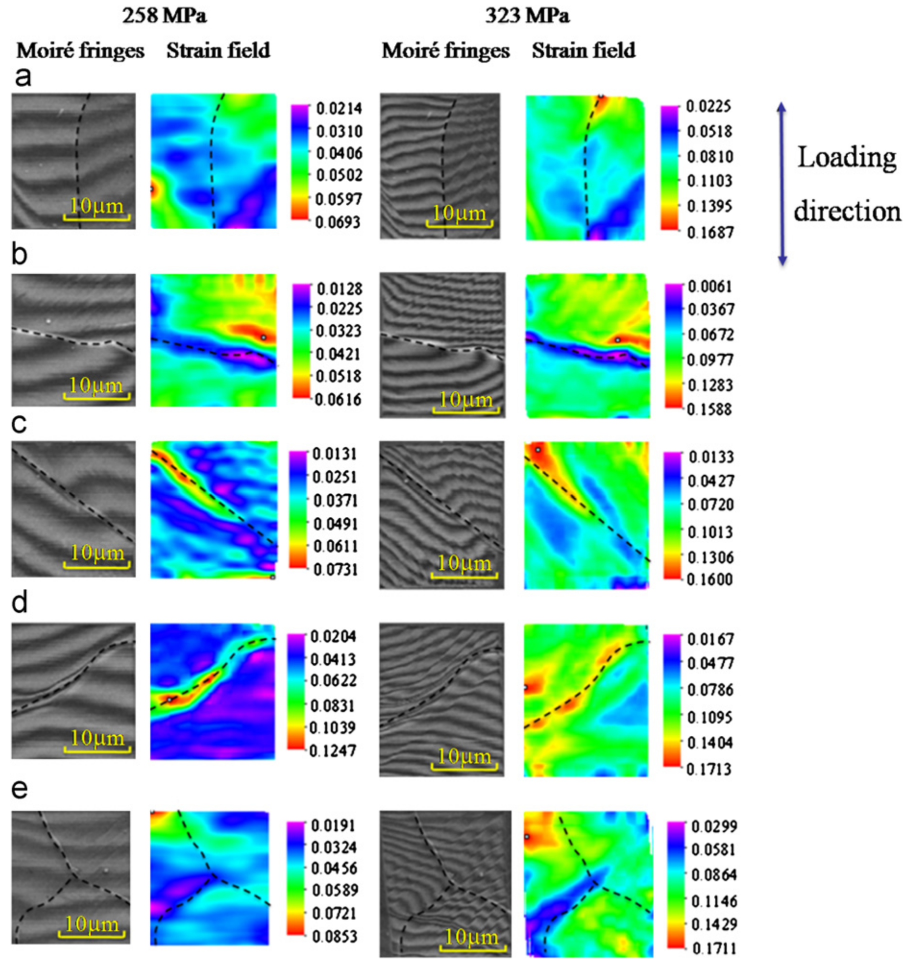

Fig. 12. Moiré fringes and strain fields around grain boundaries with different directions, each row corresponds to one type of grain boundary, where the first two images are the moiré fringes and strain field under the stress of 258 MPa while the second two images are the moiré fringes and strain field under the stress of 323 MPa, the dashed lines are grain boundaries, the dots are the locations of the maximum strain.

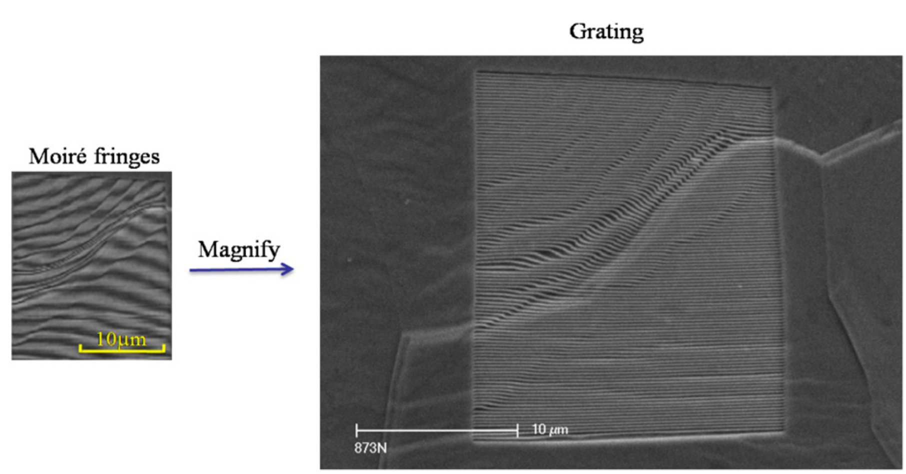

Fig. 13. Moiré fringes and grating corresponding to Fig. 12(d) under stress of 323 MPa.

Acknowledgment

The authors are grateful to the financial supported by the National Basic Research Program of China ("973" Project) (Grant nos. 2010CB631005, 2011CB606105), the National Natural Science Foundation of China (Grant nos. 90916010, 11172151), Specialized Research Fund for the Doctoral Program of Higher Education (Grant no. 20090002110048). A lot thanks to Manqiong Xu for offering the specimen material and Zhenxing Hu for helpful discussions on random phase shifting moiré method. The authors are grateful to Prof. Zhaoyang Wang for offering his processing software of moiré fringes.

References

[1] Zhang N, Tong W. An experimental study on grain deformation and interactions in an Al-0.5% Mg multicrystal. Int J Plast 2004;20:523–42.
[2] Carroll J, Abuzaid W, Lambros J, Sehitoglu H. An experimental methodology to relate local strain to microstructural texture. Rev Sci Instrum 2010;81: 083703.
[3] Kang YL, Zhang ZF, Wang HW, Qin QH. Experimental investigations of the effect of thickness on fracture toughness of metallic foils. Mater Sci Eng A 2005;394:312–9.
[4] Chen JL, Zhang XC, Zhan N. Extended digital image correlation method for micro-region deformation measurement. Sci China Technol Sci 2011;54:1–7.
[5] Schroeter BM, McDowell DL. Measurement of deformation fields in polycrystalline OFHC copper. Int J Plast 2003;19:1355–76.
[6] Guo ZQ, Xie HM, Liu BC, Dai FL, Chen PW, Zhang QM, et al. Study on deformation of polycrystalline aluminum alloy using moire interferometry. Exp Mech 2006;46:699–711.
[7] Kishimoto S, Egashira M, Shinya N. Microcreep deformation measurements by a moire method using electron beam lithography and electron beam scan. Opt Eng 1993;32:522–6.
[8] Kishimoto S, Shinya N, Mathew M. Application of electron beam lithography to study microcreep deformation and grain boundary sliding. J Mater Sci 1997;32:3411–7.
[9] Post D, McKelvie J, Tu M, Dai F. Fabrication of holographic gratings using a moving point source. Appl Opt 1989;28:3494–7.
[10] Kishimoto S, Tanaka Y, Yin F, Kagawa Y, Nagai K. Strain distribution measurement in laminated martensitic/austenitic steel during a compressive test by the electron moire method. J Strain Anal Eng Des 2011;46:1–6.
[11] Tang MJ, Xie HM, Zhu JG, Li XJ, Li YJ. The study of moiré grating fabrication on metal samples using nanoimprint lithography. Opt Express 2012;20: 2942–55.
[12] Xie HM, Li YJ, Du H, Pan B, Luo Q, Gu CZ, et al. The technique for fabricating submicron moire grating using FIB milling. Adv Mater Res 2008;47:710–3.
[13] Li Y, Xie H, Guo B, Luo Q, Gu C, Xu M. Fabrication of high-frequency moiré gratings for microscopic deformation measurement using focused ion beam milling. J Micromech Microeng 2010;20:055037.
[14] Wang ZY. Development and application of computer-aided fringe analysis. Mechanical engineering.University of Maryland; 2003 pp. 53–66.
[15] Xie HM, Shang HX, Dai FL, Li B, Xing YM. Phase shifting SEM moire method. Opt Laser Technol 2004;36:291–7.
[16] Wang ZY, Han B. Advanced iterative algorithm for randomly phase-shifted interferograms with intra-and inter-frame intensity variations. Opt Laser Eng 2007;45:274–80.
[17] Wang ZY, Han B. Advanced iterative algorithm for phase extraction of randomly phase-shifted interferograms. Opt Lett 2004;29:1671–3.
[18] Hu ZX, Xie HM, Lu J, Liu ZW, Wang QH. A new method for the reconstruction of micro-and nanoscale planar periodic structures. Ultramicroscopy 2010; 110:1223–30.
[19] Wang QH, Xie HM, Hu ZX, Zhang J, Sun J, Liu G. Residual thermo-creep deformation of copper interconnects by phase-shifting SEM moiré method. Appl Mech Mater 2011;83:185–90.
[20] Durelli A, Parks V. Moire analysis of strain. Englewood Cliffs, NJ: Prentice-Hall; 1970.
[21] Tseng A. Recent developments in micromilling using focused ion beam technology. J Micromech Microeng 2004;14:R15–34.
[22] Reyntjens S, Puers R. A review of focused ion beam applications in microsystem technology. J Micromech Microeng 2001;11:287–300.